The International Journal of Advanced Manufacturing Technology (2020) 108:345–356
https://doi.org/10.1007/s00170-020-05138-8

ORIGINAL ARTICLE

Influence of carbon content on the martensitic transformation of titanium stabilized austenitic stainless steels

Juan Manuel Pardal[1,2] · Sérgio Souto Maior Tavares[1,2] · Mauro Teixeira Tavares[1] · Pedro Soucasaux Pires Garcia[2] · Javier Alejandro Carreno Velasco[3] · Hamilton Ferreira Gomes Abreu[4] · Juan Pablo Pardal[5]

Received: 5 November 2019 / Accepted: 24 February 2020 / Published online: 14 May 2020

Abstract

Austenitic stainless steels (ASS) are corrosion resistant alloys in which the desirable mechanical properties may be attained by cold working in the final stages of the fabrication process. This manufacturing process may induce martensitic transformation from the austenitic phase, where the chemical composition plays an important role as it influences the stacking fault energy (SFE). Therefore, this work evaluated the influence of carbon content on martensitic transformation of Ti stabilized ASS. Thus, the austenite transformed into martensite by cold rolling was observed by Light Optical Microscopy (LOM) and quantified by Vibrating Sample Magnetometer (VSM), and X-Ray Diffraction (XRD) for Ti stabilized ASS with different carbon contents. The experimental results about the martensitic transformation behavior for each alloy were compared with previous results on other ASS and Duplex Stainless Steel (DSS), tested in similar conditions, verifying a high correlation with a sigmoidal model previously applied in these alloys. Additionally, it was carried out a SFE analysis, estimated by thermodynamic model, corroborating that the alloy's carbon content has a strong influence on the material's stability. Finally, it was observed a sudden increase in microhardness value as a consequence of the high amount of austenite transformed into martensite at very low strains that might affect the steels performance in several applications.

Keywords Austenitic stainless steels · Cold rolling · Martensitic transformation · Magnetic properties · Microhardness

✉ Juan Manuel Pardal
juanpardal@id.uff.br

Sérgio Souto Maior Tavares
ssmtavares@id.uff.br

[1] Programas de Pós-Graduação em Engenharia Mecânica (PGMEC) e Montagem Industrial - Rua Passo da Pátria, Universidade Federal Fluminense (UFF), 156, CEP 24210-240, Niterói, RJ, Brasil

[2] Programa de Pós-Graduação em Engenharia Mecânica e Tecnologia de Materiais, Centro Federal de Educação Celso Suckow, Rio de Janeiro, RJ, Brasil

[3] Laboratório de H_2S, CO_2 e Corrosividade, Instituto Nacional de Tecnologia (INT), Rio de Janeiro, RJ, Brasil

[4] Departamento de Engenharia Metalúrgica e de Materiais, Universidade Federal do Ceará (UFC), Centro de Tecnologia, Fortaleza, CE, Brasil

[5] Departamento de Ingeniería Mecánica, Facultad Regional Avellaneda, Universidad Tecnológica Nacional (UTN), Buenos Aires, Argentina

1 Introduction

Austenitic stainless steels (ASS) are corrosion resistant alloys widely used as bars, wires, pipes, and even pressure vessels, such as cryogenic reservoirs and reactors [1–3]. In this stainless steel family, the final adjustment of mechanical properties and dimensional control are achieved by drawing, bending, cold rolling, and stretching processes [4–6]. However, in these mechanical processes, the austenite phase (γ-FCC) can undergo martensitic transformations by diffusionless shear mechanism. The two martensitic structures reported in the literature of ASS are [7] ϵ (HCP and paramagnetic) and alpha prime (α') (BCC and ferromagnetic). This phenomenon can also happen during service life of equipment such as piping and vessels, mainly due to cyclic loads in conditions where localized deformation ends up provoking damage accumulation. These strains, added to that originated from the manufacturing processes, may result in a premature failure in this stainless steels family [8, 9].

It is also important to state that metallurgical variables such as grain size [10] and texture [11] can influence the martensitic transformation. However, it is commonly accepted that the stacking faults in austenite phase are preferential sites for martensite formation. Therefore, the stacking fault energy (SFE) is a key parameter in the evaluation of the deformation-induced martensite (DIM) phenomenon [12–14]. In general, the susceptibility for martensite formation, or the metastability of austenite, increases with the decrease of SFE. It is also common that austenitic stainless steels with low SFE values exhibit small fractions of ϵ martensite, and this phase can also be present when the material is subjected to a small level of plastic strain. In these steels, when increasing the absolute true strain values, the amount of ϵ martensite reaches a maximum value and then decreases, while the amount of α' martensite increases continuously. Considering the aforementioned fact, it was suggested a sequence of transformation consisting of $\gamma \rightarrow \epsilon \rightarrow \alpha'$, but the direct transformation $\gamma \rightarrow \alpha$' can also happen, such as reported recently by Tiamiyu et al. [10] in a compressed AISI 321 austenitic stainless steel. In austenitic Fe-Mn-Al alloys, the transformation $\gamma \rightarrow \epsilon \rightarrow \alpha$' occurs with SFE values under 20 mJ/m^2, while the direct transformation $\gamma \rightarrow \alpha'$ takes place for SFE greater than 20 mJ/m^2 [15]. Therefore, some previous researches had correlated the SFE (mJ/m^2) to the chemical composition (% in wt.) for ASS. Some examples of equations proposed in the literature are listed below [16–18].

$$\mathrm{SFE} = -53 + 6.2\mathrm{Ni} + 0.7\mathrm{Cr} + 3.2\mathrm{Mn} + 9.3\mathrm{Mo} \quad (1)$$

$$\mathrm{SFE} = 25.7 + 2\mathrm{Ni} + 410\mathrm{C} - 0.9\mathrm{Cr} - 77\mathrm{N} - 13\mathrm{Si} - 1.2\mathrm{Mn} \quad (2)$$

It is important to note that Eq. 2 suggests a significant influence of carbon content in the SFE calculation. This result was also reported by Yang et al. [19], where the authors also found a strong dependence of the SFE with carbon content for several austenitic stainless steels grades. Furthermore, Tsuchida et al. [20] proposed the use of $\mathrm{Ni_{eq}}$ as a parameter to evaluate the transformation-induced plasticity (TRIP) effect in metastable ASS, and observed that the volume fraction of austentite transformed into martensite increased with lowering Ni content. Thus, Kang et al. [21] reassessed the latest proposed $\mathrm{Ni_{eq}}$ equations and proposed a new modified relation based on grades 304, 304L, 316, and 316L ASS, taking into account a more accurate nitrogen effect, as can be stated in Eq. 3. Besides that, these authors suggested that a $\mathrm{Ni_{eq}^{mod}}$ should be taken as a lower limit for applications involving hydrogen.

$$\mathrm{Ni_{eq}^{mod}} = \mathrm{Ni} + 0.65\mathrm{Cr} + 1.05\mathrm{Mn} + 0.98\mathrm{Mo} + 0.35\mathrm{Si} + 12.6\mathrm{C} + 33.6\mathrm{N} \quad (3)$$

On the other hand, the initial temperature for martensitic transformation (M_s), in K, can also be correlated to the chemical composition (% in wt.) using Eqs. 4–6 [17] as well as Eq. 7 [22]:

$$M_s = 1578 - 41.7\mathrm{Cr} - 61.1\mathrm{Ni} - 33.3\mathrm{Mn} - 27.8\mathrm{Si} - 1670(\mathrm{C} + \mathrm{N}) \quad (4)$$

$$M_s = 1455 - 36.7\mathrm{Cr} - 56.7\mathrm{Ni} - 1460(\mathrm{C} + \mathrm{N}) \quad (5)$$

$$M_s = 1755 - 47\mathrm{Cr} - 59\mathrm{Ni} - 54\mathrm{Mn} - 37\mathrm{Si} - 2390\mathrm{C} - 3720\mathrm{N} - 56\mathrm{Mo} - 180\mathrm{Ti} - 14\mathrm{Co} \quad (6)$$

$$M_s = 1350 - 1665(\mathrm{C} + \mathrm{N}) - 28Si - 33\mathrm{Mn} - 42\mathrm{Cr} - 61\mathrm{Ni} \quad (7)$$

Finally, it is possible to estimate the chemical driving force ($\Delta G^{\gamma \rightarrow \alpha'}$(T)) for stable α'-nuclei from γ embryos, such as reported by Behjati et al. [15] for Fe-Cr-Ni pure alloys and Moallemi et al. [23] for AISI 201 ASS. These estimations take into account other important elements such as C, N, Mn, Mo, and Si. These works were based on the expression first proposed by Kaufman for ternary solid solution of Fe-Cr-Ni system, presented in Eq. 8, where X_{Cr} and X_{Ni} are mole fractions of Cr and Ni, respectively:

$$\begin{aligned}\Delta\ G^{\gamma \rightarrow \alpha'}(T) &= 2.43T(1 - \ln(T)) - 26040X_{\mathrm{Cr}}X_{\mathrm{Ni}} \\ &+X_{\mathrm{Ni}}(-15540 + 2.97 \times 10^{-3}T^2 + 1.64 \times 10^{-7}T^3) \\ &+X_{\mathrm{Cr}}(1932 + 4.2 \times T) \\ &+X_{\mathrm{Ni}}(1 - X_{\mathrm{Cr}} - X_{\mathrm{Ni}})(15120) \\ &+X_{\mathrm{Cr}}(1 - X_{\mathrm{Cr}} - X_{\mathrm{Ni}})(-11760 + 3.15T) \\ &+(1 - X_{\mathrm{Cr}} - X_{\mathrm{Ni}})(5048.4 - 1.01 \times 10^{-2}T^2 \\ &+6.46 \times 10^{-6}T^3)\end{aligned} \quad (8)$$

It is common to estimate the chemical driving force for the transformation at the M_s absolute temperature ($\Delta G^{\gamma \rightarrow \alpha'}(M_s)$), and Eq. 8 can also be used to estimate the phase equilibrium absolute temperature (T_0), by simply making $\Delta G^{\gamma \rightarrow \alpha'}(T_0) = 0$. Saeedipour et al. [24] analyzed the driving force variation between room and M_s temperatures versus nitrogen content for AISI 201 ASS, observing that the driving force decreases with nitrogen content. According to Curtze et al. [25] and other authors [23, 26], a SFE can also be estimated by thermodynamic approach (SFE_T) taking into account the following Eq. 9:

$$\mathrm{SFE}_T = 2\rho\Delta G^{\gamma \rightarrow \alpha'} + 2\sigma \quad (9)$$

where

ρ: Molar surface density
σ: γ/α' interfacial energy

Nevertheless, there were found many works to estimate the SFE in the literature, all of which were based only on the chemical composition of the alloys, such as those presented for M_s temperature. Das, [27] made a thorough literature review about this subject, and reported many disagreements between previously published works, especially when comparing alloys with different compositions. The author stated that due to lack of experimental data, however, further works on the effect of C on the SFE for other alloys still needs to be carried out. Similarly, the effect of Mn is also ambiguous, as already shown in Eqs. 1 and 2. It can then be concluded that there is still a lack of consistent experimental data. Nevertheless, in a recent research, Ogawa et al. [28] observed that carbon content affects stabilization of austenite phase as well as the tendency to form DIM.

Some other interesting aspects related to martensite characterization techniques were analyzed by Beese and Mohr [29] in an AISI 301 LN ASS, and more recently by Shirdel et al. [30] in an AISI 304L austenitic grade. These authors concluded that micrography, basic X-ray diffraction and EBSD techniques all provides good qualitative results, but the absolute error in the estimation of martensite content can be greater than 10%. However, the inaccuracies associated with metallographic surface preparation can be eliminated when using magnetic measurements, once they give the bulk mean value of the martensite content over a relatively large volume. Several previous works [31–34] have addressed the martensitic transformation by cold rolling in ASSs, lean duplex, and duplex stainless steels (DSSs). In their work, the α' martensite volume fraction was quantified using a vibrating sample magnetometer (VSM) to measure the saturation magnetization of the samples. Then, the amount of austenite transformed into martensite was correlated with the true strain applied, according to the sigmoidal function presented in Eq. 10 [33, 34].

$$C_{\alpha'} = C_s \times \exp(-\exp(-n(\epsilon - K))) \quad (10)$$

where

$C_{\alpha'}$: Volumetric fraction of α'
C_s: Saturation value for the martensite volume fraction
n: Constant related to the transformation rate
ϵ: True strain
K: Time constant, related to the initial stage of transformation

The interest on studies about the susceptibility of ASSs to martensitic transformation is due to the great influence of this transformation on mechanical, chemical, and physical properties of these steels. For instance, the formation of DIM was found to decrease the corrosion resistance of ASSs [35, 36]. On the other hand, Jha et al. [8] studied the failure of an AISI 321 ASS pipeline in a qualification test, where a crack occurred in the bent portion of the cold worked pipe. In the latter case, the combination of low temperature with the presence of DIM during loading dramatically decreased the material's toughness, which eventually led to the failure. The austenitic stainless steel grade AISI 321 is a Ti-stabilized alloy commonly selected to perform services in temperatures as high as 800 °C [37], but it can also be found operating in low temperature applications. Hence, products made of this alloy might exhibit different carbon contents, up to 0.08% (% wt.). Nevertheless, nowadays it is possible to find some steel manufacturers that produce Ti-stabilized ASS with extra low carbon, resulting in a cheaper product due to technological and economical advances in the refining process that will require less amounts of Ti for stabilizing purposes. A direct consequence of this reduction in carbon content, even if it does not change the classification in its ASTM steel grade, is that the austenitic microstructure will become more unstable, making it easier to transform once plastic strain is applied. Therefore, this work evaluated the influence of the carbon content on the susceptibility to martensitic transformation in three AISI 321 ASSs.

2 Materials and methods

In this study, there were analyzed three different pipe heats delivered under specification AISI grade 321, where the major differences between each heat was the carbon and Ti contents. Thus, the samples removed from the pipes were identified as low carbon (LC), medium carbon (MC), and high carbon (HC). The Ti content varies as a function of the carbon fraction as provided in ASTM A312 for stabilization purposes. Table 1 shows the chemical compositions of the three steels studied in this work.

The samples were cut from the pipes, pressed and machined in order to obtain small specimens with 15.0 mm × 10.0 mm × 3.2 mm. Hereafter, all samples were solution treated in inert atmosphere at 1373 K for 40 min followed by water cooling to room temperature. Then, they were cold rolled at room temperature so that to apply different true strains (ϵ) values, which were calculated using Eq. 11, where t_0 and t_f are the values for initial and final thickness, respectively. The rolling direction, temperature,

Table 1 Chemical composition of austenitic stainless steels (ASS) as received from studied

Id	(%wt.) (Fe in balance)									
	Cr	Ni	Mn	Si	Ti	C	S	P	Mo	N
LC	17.11	9.22	0.85	0.52	0.10	0.015	0.002	0.03	0.06	0.01
MC	17.16	9.08	1.50	0.41	0.38	0.035	0.009	0.02	-	0.02
HC	17.53	9.79	1.65	0.30	0.45	0.064	0.006	0.03	0.32	0.01

and strain rate were carefully maintained constant to avoid some influences of these parameters in the martensitic transformation kinetics, such as recommended by Tiamiyu et al. [10] and Abedi and Serajzadeh [38]. Table 2 correlates the samples identifications with their respective thickness and absolute true strain value. Additionally, a HC sample was was immersed in liquid nitrogen (77 K) for approximately 2 minutes before each rolling pass. This specimen, called HCN, was strained at 3.82 true strain (in absolute value), as to obtain a 100% martensitic structure.

$$\epsilon = \ln(\frac{t_0}{t_f}) \tag{11}$$

After rolling, small specimens were cut with diamond disc by precision sectioning, employing low RPM and load to avoid edges deformation. These specimens were taken for magnetic analysis in the vibrating sample magnetometer (VSM), where magnetization curves were obtained using a maximum applied magnetic field (H) of 1.5T. The values of saturation magnetization (m_s) of each specimen were obtained by linear extrapolation to $H = 0$ in the M x H curve, from magnetization (M) values acquired close to the maximum applied magnetic field, in order to establish a comparative study with previous works in different stainless steels [9, 30, 32, 37]. In these works, there were estimated values for intrinsic saturation magnetization (m_{si}) corresponding 100% of austenite transformed into martensite for each alloy. After this, it is possible to determinate the martensite volumetric fraction (MVF) in terms of deformation by dividing the m_s value applied by the alloy's m_{si} value.

Table 2 Identification of samples as a function of the absolute true strain value ($|\varepsilon|$)

$\|\varepsilon\|$	Specimen Identification		
	LC	MC	HC
0.00	LC-0.00	MC-0.00	HC-0.00
0.09	LC-0.09	MC-0.09	HC-0.09
0.17	LC-0.17	MC-0.17	HC-0.17
0.33	LC-0.33	MC-0.33	HC-0.33
0.52	LC-0.52	MC-0.52	HC-0.52
0.76	LC-0.76	MC-0.76	HC-0.76
1.01	LC-1.01	MC-1.01	HC-1.01
1.26	LC-1.26	MC-1.26	HC-1.26
1.64	LC-1.64	MC-1.64	HC-1.64
2.01	LC-2.01	MC-2.01	HC-2.01
2.29	LC-2.29	MC-2.29	HC-2.29
2.77	-	MC-2.77	HC-2.77
3.20	-	MC-3.20	HC-3.20
3.68	-	-	HC-3.68

Some selected specimens of each heat were prepared for light optical microscopy (LOM) analysis in order to evaluate the rolled surface. The metallographic preparation was made by grinding and polishing using an automatic polisher with controlled speed, force, and time of exposure. Then, it was applied an electrolytic etching with a 10% oxalic acid solution (9 V, 30 s) for LOM comparative observation at same true strain values between studied alloys. Besides, some selected samples were also analyzed by X-ray diffraction (XRD) in a Brucker diffractometer, where LC-0.00, LC-0.33, and LC-2.29 samples were performed with CoKα (1.7890 Å) radiation, 35 kV, and 40 mA, without monocromator, for an angular interval of 45°–110° in step scan mode with step size of 0.01° at room temperature. Different phase quantification methods were performed in these conditions. The presence of ϵ martensite was not considered, since it was only detected in a very small amount in sample LC-0.00, close to the accuracy limit of XRD analysis. The first semi-quantitative method employed in the analysis was the reference intensity ratio (RIR), using the X'Pert Highscore 1.0 software. The RIR of austenite and martensite were considered as 7.97 and 10.77 in this analysis, according to PDF 03-065-4150 and PDF 03-065-4899 reference cards, respectively [39, 40]. Furthermore, the next method employed was the direct comparison (DC) proposed by Cullity [41] where all austenite and martensite peaks were compared taking into account equal scattering factors for both phases [31, 42]. The last method was the Rietveld refinement method (RR) quantitative analysis, performed with the *Full Prof-suite* software [43]. In this last case, cif files of austenite and martensite were obtained from ICSD—Inorganic Crystal Structure Database [44]. A pseudo-Voigt profile function

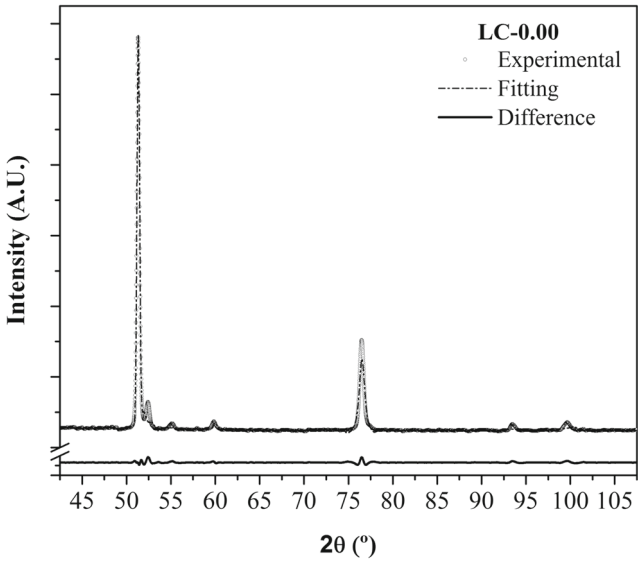

Fig. 1 Rietveld refinement of LC-0.00 condition

was adopted for this analysis, and linear interpolation between a set background points with refinable heights was taken into account. March's modified correction was employed in the refinement process, minimizing texture effects, such as reported by Haušild et al. [45]. Thus, several factors such as phase scale, cell lattice parameters, full width at half maximum (FWHM), and shape parameters were carefully refined by least squares, so that the model attained χ^2 values less than 1.5 for all cases. It was observed a good correlation between the experimental values and model fittings for all studied samples, as shown in Fig. 1 for LC-0.00 condition. Additionally, highly strained samples MC-3.20 and HCN-3.82 were also analyzed by XRD, with CuKα (1.5840 Å) radiation, 40 kV and 40 mA, without monocromator, with an angular interval 40°–110° in step scan mode, with step size 0.01° at room temperature.

After ascertain the values of m_s that correspond to the 100% volume fraction martensite, it is possible to calculate the values of $C_{\alpha'}$. Hence, Eq. 10 can be linearized to Eq. 12 and plotted in order to obtain the values of n and K.

$$\ln\left(\ln(\frac{C_{\alpha'}}{C_s})\right) = -n\epsilon + \mathrm{nK} \tag{12}$$

It is also interesting to evaluate the transformation rate, and that can be achieved by deriving the Eq. 11 in respect to the true strain ϵ, as shown in Eq. 13 [33].

$$\frac{dC_{\alpha'}}{d\epsilon} = (\mathrm{ne}^{-n(\epsilon-K)}) \times (C_s e^{-e^{-n(t-K)}}) \tag{13}$$

Finally, some specimens were prepared by electropolishing for microhardness Vickers tests with 9.8N load for 15 s.

Table 3 Calculated SFE for the three alloys studied

Id	%C	SFE (mJ/m^2)		SFE$_c$ (mJ/m^2)	Influence of C in the SFE (%)
		Eq. 1	Eq. 2	Eq. 2	
LC	0.015	19.45	25.91	6.05	23.35
MC	0.035	20.11	34.40	14.35	41.72
HC	0.064	28.23	49.26	26.32	53.43

3 Results and discussion

First, some compositional features of the ASS must be highlighted. As stated before, MC and HC alloys are in accordance with requirements of ASTM 312 Types 321 and 321H, respectively. The LC alloy is not in accordance to the specification for grade AISI 321 in the latest edition of the standard because its Ti content is slightly lower than five times of its C+N content, which is necessary for an effective performance in high temperature services. Table 3 shows the SFEs calculated for the three alloys using Eqs. 1 and 2. Equation 1 does not include the effect of carbon, and its contribution is highlighted in Table 3 in the column SFE$_C$, which was calculated using Eq. 2. Table 4 shows the M_s values calculated with Eqs. 4, 5, and 6. Quite different results were obtained with the three equations, but it is clear that the M_s decreases with the increase of carbon content.

The chemical driving force in LC, MC, and HC alloys were calculated using Eq. 8, where X_{Ni} and X_{Cr} were determined from niquel equivalent (Ni$_{\mathrm{eq}}$) and chromium equivalent (Cr$_{\mathrm{eq}}$), based on the following expressions [46].

$$\mathrm{Cr_{eq}} = \mathrm{Cr} + 1.37\mathrm{Mo} + 1.5Si + 2.0\mathrm{Nb} + 3.0\mathrm{Ti} \tag{14}$$

$$\mathrm{Ni_{eq}} = \mathrm{Ni} + 0.3\mathrm{Mn} + 22C + 14.2\mathrm{N} + \mathrm{Cu} \tag{15}$$

Table 5 shows the driving force values calculated at M_s temperature using Eqs. 7 and 8, as well as the results from a thermodynamic approach presented in equation (9) to estimate the stacking fault energy (SFE$_T$) assuming σ and ρ values as 8 mJ/m^2 and 2.96 × 10 − 05 mol/m^2, respectively [25]. The equilibrium temperature (T_0) values

Table 4 M_s Temperatures for the three alloys studied

Id	M_s (K)			
	Eq. 4	Eq. 5	Eq. 6	Eq. 7
LC	210.2	262.3	241.7	251.2
MC	161.1	235.9	115.4	202.5
HC	64.0	150.5	-	105.5

Table 5 Chemical driving force ($\Delta G^{\gamma\rightarrow\alpha'}(M_s)$), thermodynamically calculated SFE_T and Ni_{eq}^{mod} values for LC, MC, and HC alloys

Id	$\Delta G^{\gamma\rightarrow\alpha'}(M_s)$ (J/mol)	SFE_T (mJ/m^2)	T_0 (K)	Ni_{eq}^{mod}
LC	− 1150.3	26.12	647.5	22.14
MC	− 1059.3	27.97	606.6	22.93
HC	− 908.7	32.63	519.7	24.43

are also reported in Table 5, where it can be observed that the austenite becomes more stable with the increase of carbon content. In this table, it was also added the values of modified niquel equivalent (Ni_{eq}^{mod}) proposed by Kang et al. [21]. Even though it consists in a model based in the 304, 304L, 316, and 316L ASS composition, it can be used as a reasonably accurate parameter for comparison purposes. It is important to note that the Ni_{eq}^{mod} differs from the other models by taking the nitrogen instead of carbon as the major element responsible for the stabilization of the austenitic phase. Table 1 indicates that the BC and MC alloys nitrogen content are about the double as that of the HC alloy. Nevertheless, the results presented at Table 5 indicates that LC alloy are the less stable followed by the MC and HC, the last being the most stable due their respective Ni_{eq}^{mod} values.

Figure 2 shows the influence of each element estimated by equation (9). The curves were obtained by varying a single element at a time (from the minimum content present among the LC, MC, and HC samples to the maximum), while keeping the other variables constant. The base composition used was that of LC samples. Here, it becomes clear that the variation in the carbon content is responsible for the larger range of SFE_T values.

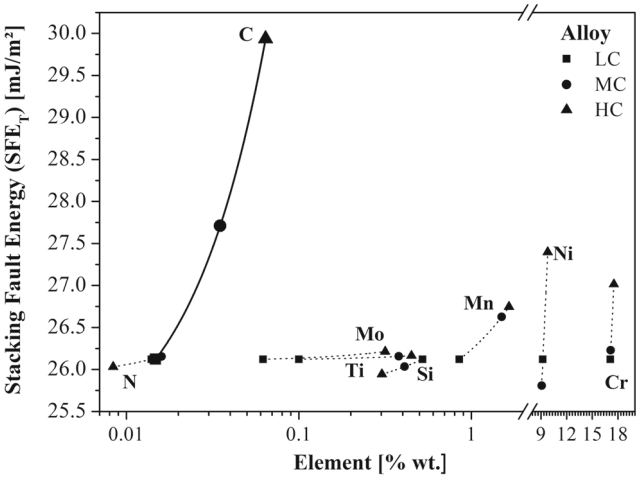

Fig. 2 SFE_T versus %wt. of each element present in the thermodynamic model

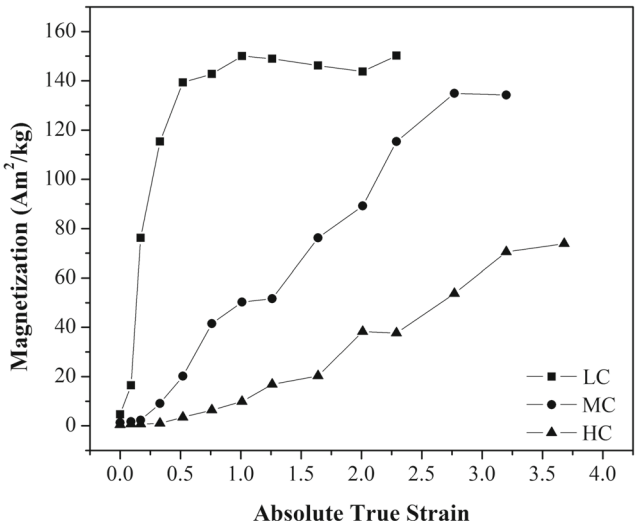

Fig. 3 Saturation magnetization (m_s) versus absolute true strain ($|\epsilon|$) for LC, MC, and HC ASS

Figure 3 exhibit the values of saturation magnetization (m_s) versus absolute true strain ($|\epsilon|$) curves of LC, MC, and HC alloys. In LC and MC specimens, the $\gamma \rightarrow \alpha'$ transformation reaches saturation, indicating that a fully martensitic microstructure was obtained through room temperature rolling. The full transformation of austenite in the MC alloy was corroborated by the XRD (Fig. 4) of the sample with 3.2 absolute true strain value (MC-3.20).

According to Fig. 3, the amount of strain necessary to provoke 100% of transformation is much lower in LC ($|\epsilon| \approx 1.0$) than in MC ($|\epsilon| \approx 2.8$). This higher$\gamma \rightarrow \alpha'$ susceptibility in the LC sample is coherent to the SFE values obtained both by Eq. 2 and by thermodynamic modeling, and it shows that the carbon content is an important

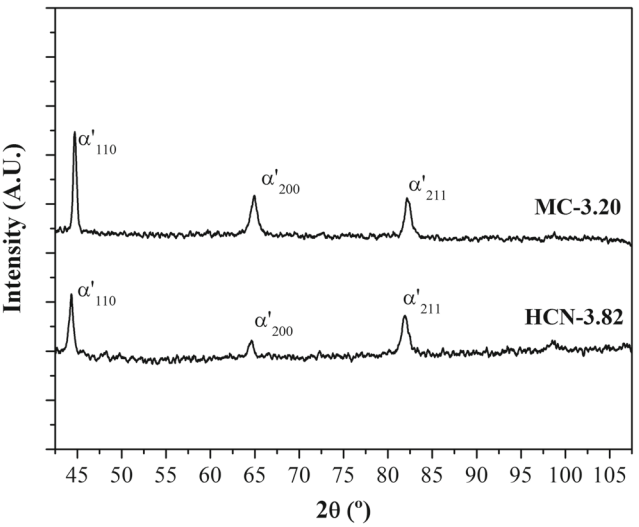

Fig. 4 Diffractograms of samples MC-3.20 and HCN-3.82

variable to evaluate austenite stability in this alloy family. Corroborating the aforementioned, it was also necessary to resort to cryogenic conditions in order to obtain 100% of martensitic transformation in the higher carbon alloy. Figure 4 also shows the diffractogram of specimen HCN with $|\epsilon| \approx 3.82$, with reflections of α' and no traces of austenite.

The m_s values corresponding to 100% of martensite are presented in Fig. 3, and are 150.2 Am^2/kg and 134.3 Am^2/kg for LC and MC alloys, respectively. These are the intrinsic saturation magnetization values (m_{si}) of martensite for LC and MC steels. The m_{si} also depends on the chemical composition, because alloying elements and impurities affect the magnetic moment of iron. The results show that m_{si} decreases with the carbon content of α' martensite. The m_{si} of HC steel martensite was 120.15 Am^2/kg, measured in the HCN specimen. Table 6 compares the m_{si} of this work with others from ASS and duplex stainless steel (DSS) available in the literature [31–34]. Hence, the martensite α' volume fraction ($C_{\alpha'}$) can be determined by the Eq. 16, according to the magnetic method described by Tavares et al. [32]:

$$C_{\alpha'} = \frac{m_s}{m_{si}} \tag{16}$$

where

m_s: Sample's saturation magnetization (Am^2/kg)
m_{si}: Alloy's intrinsic saturation magnetization (Am^2/kg)

Figure 5 shows the volume fraction of austenite transformed into martensite, or martensite volume fraction (MVF), as a function of absolute true strain ($|\epsilon|$) for LC, MC, and HC steels. The sigmoidal behavior of the curves is in agreement with previous works [33, 34].

Figures 6, 7, and 8 present the microstructures of LC, MC, and HC respectively. Comparing the samples deformed to $|\epsilon| = 0.17$ (Figs. 6b, 7b, and 8b), it is observed that

Table 6 Intrinsic saturation magnetization of the α' martensite (m_{si}) values obtained for the alloys analyzed in this work and another previously studied

Material	m_{si} (Am^2/kg)
UNS S31803 (DSS) [31]	133.0
AISI 301 LN (ASS) [32]	157.1
201 mod (ASS) [33]	140.0
UNS S32304 (lean DSS) [34]	140.2
LC	150.2
MC	134.3
HC	120.3

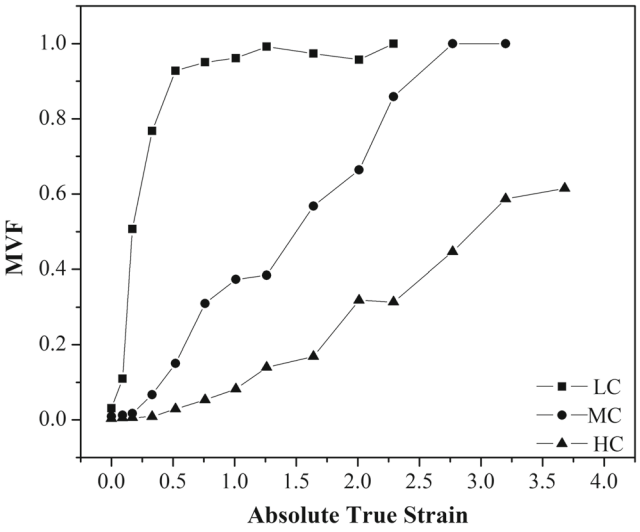

Fig. 5 Martensite volume fraction (MVF) as function of abolute true strain ($|\epsilon|$) for LC, MC, and HC ASS

the amount of martensite formed in slip bands increases from the higher to the lower carbon alloy, according to the previous results based on magnetic method. None of the three alloys exhibited traces of delta ferrite (δ).

It can be noted from Figs. 6a, 7a, and 8a that the samples LC, MC, and HC presented a similar austenitic grain size in the solution treated (un-deformed) condition. A detailed observation of these samples reveals that the LC steel formed some α' at slip bands, as indicated in Fig. 6a, while the other steels have only clean austenite grains and twins. The amount of α' martensite quantified in LC-0.00 sample by magnetic method was 3.12%, which seems to be much less than that can be observed in Fig. 6a. This discrepancy is a consequence of the mechanical polishing process during the metallographic preparation, which has induced martensitic transformation in the metastable LC steel. The XRD analysis of samples LC-0.00, LC-0.33, and LC-2.29 are presented in Fig. 9, where the evolution of α' peaks can be appreciated. A small peak of ϵ martensite was also present in the LC-0.00 condition. The values obtained for the phase quantification using the RIR, DC, and RR methods were 40.00%, 47.30%, and 49.35% respectively, but despite being more consistent with the microstructure presented in Fig. 6a, are in great contrast with the 3.12% obtained by magnetic method. According to Beese [40] and Talonen et al. [42], even when using fitting methodologies in XRD diffractograms, the texture effects might not be completely eliminated. It is also important to state that the penetration depth of the X-ray is restricted to the surface and sub-surface regions of the samples. In addition, it was observed [42] that the martensite content is higher on the surface than in the interior of the steel. Thus, unstrained low carbon samples LC-0.00 and those slightly

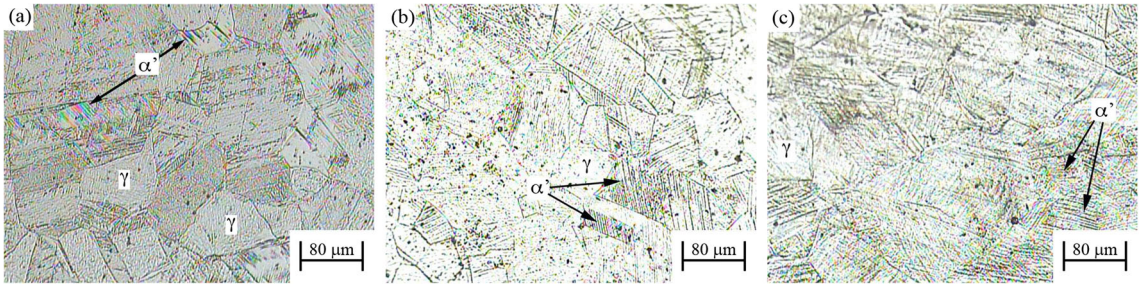

Fig. 6 Microstructures of LC ASS. **a** LC-0.00, **b** LC-0.17, and **c** LC-0.33

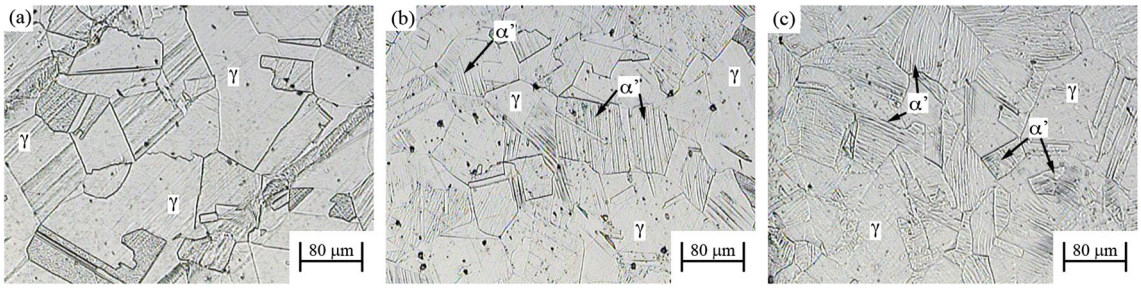

Fig. 7 Microstructures of MC ASS. **a** MC-0.00, **b** MC-0.17, and **c** MC-0.33

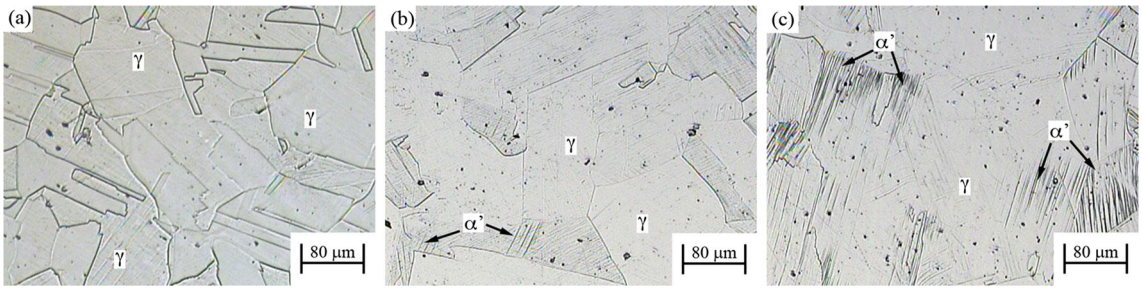

Fig. 8 Microstructures of HC ASS. **a** HC-0.00, **b** HC-0.17, and **c** HC-0.33

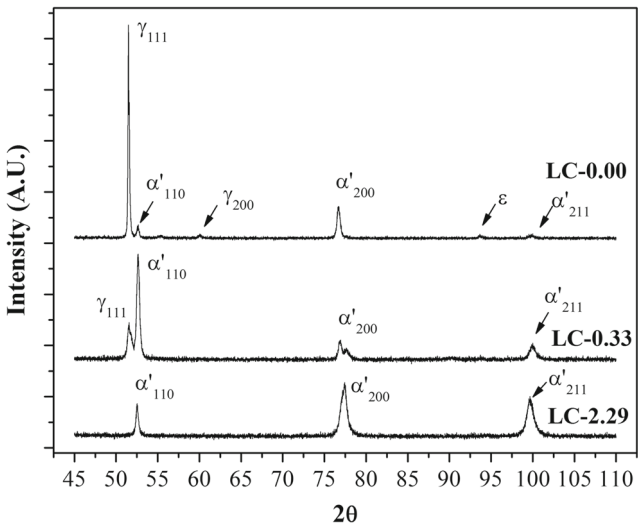

Fig. 9 X-ray diffractograms of LC samples with true strains − 0.00, − 0.33, and − 2.29

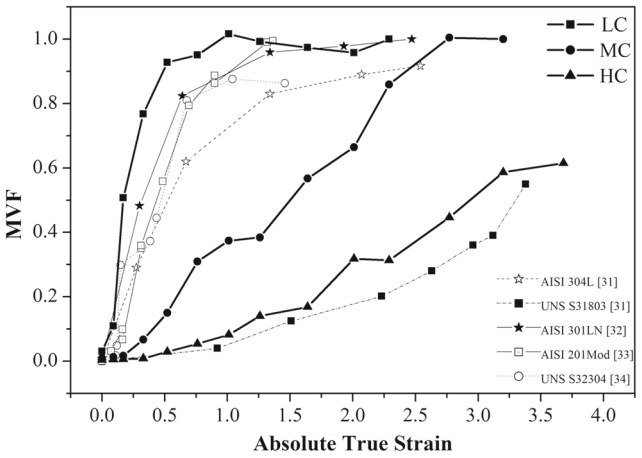

Fig. 10 Martensite volumetric fraction (MVF) versus absolute true strain for different stainless steels in comparison with LC, MC, and HC studied

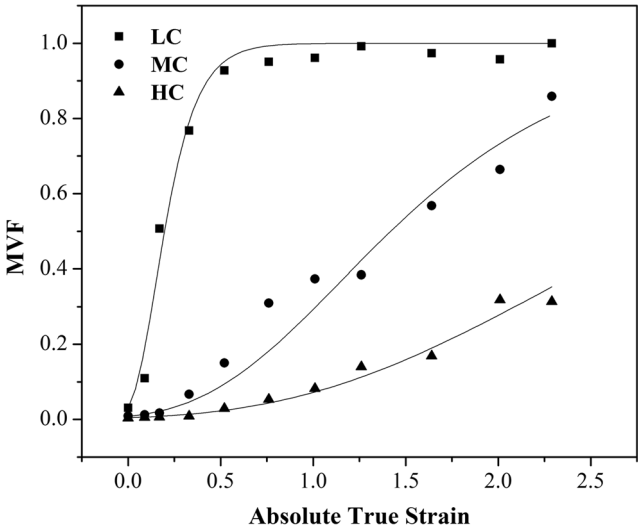

Fig. 11 Kinetic modeling (straight lines) for the martensitic transformation, plotted with the experimental values (dots) for comparison

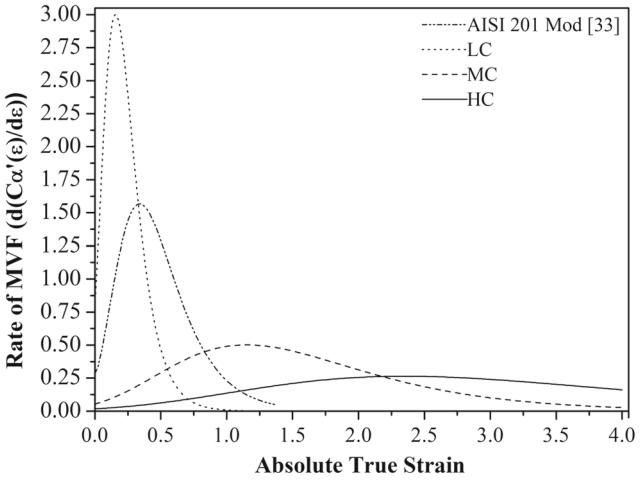

Fig. 12 Rate of MVF versus absolute true strain for the studied samples. AISI 201 Mod data [33] was added for comparison purposes

deformed are expected to present higher martensite amounts at their surfaces, due to mechanical preparation and non uniformities at initial stages of rolling processes, besides the strain hardening effect at surface layers. On the other hand, the amount of α' martensite quantified for the LC-0.33 sample by magnetic method was of 76.77%, which is in agreement to Fig. 6c. In this case, the phase quantification by RIR (80.00%), DC (71.81%), and RR (65.91%) methods are close to the magnetic method result, as the deformations in this sample was more uniform along the material's cross section. Figure 10 shows the martensite volume fraction (MVF) versus absolute true strain curves for different stainless steels. The results of LC, MC, and HC obtained in this work were added for comparison. The kinetics behavior of LC ASS is similar to AISI 301LN, while HC ASS is close to DSS UNS S31803. In the other hand, the result obtained for the martensitic transformation model using equation (10) is presented at Fig. 11. Table 7 shows the values obtained for the n and K parameters, as well as the R^2 obtained by fitting.The n and K parameters are functions of the chemical composition, where in this case is mainly affected by carbon content, as can be noted in Table 7. In fact, Behjati and Najafizadeh [15] presented in their work a similar model to predict the martensite fraction depending on the difference between the chemical driving force calculated at M_s and at a given temperature, and both parameters proposed by the authors were also dependent on the chemical composition. Therefore, Fig. 12 presents the results for the kinetic modeling using Eq. 13. In this Figure, the rate of MVF for the AISI 321 obtained in the present work was compared to the results for the AISI 201 mod. previously analyzed by Tavares et al. [33], whose experimental values were also presented in Fig. 10. It is clear that the 201 mod. has an intermediate behavior between the LC and MC AISI 321 alloys.

Figures 13 and 14 present the microhardness variation versus absolute true strain values for the studied alloys.

Table 7 Calculated parameters for the kinetic modeling of the samples in the present work

Id	Equation 10 and correlation coefficients		
	n	K	R^2
LC	8.66	0.15	0.98
MC	1.28	1.07	0.97
HC	0.68	2.38	0.99

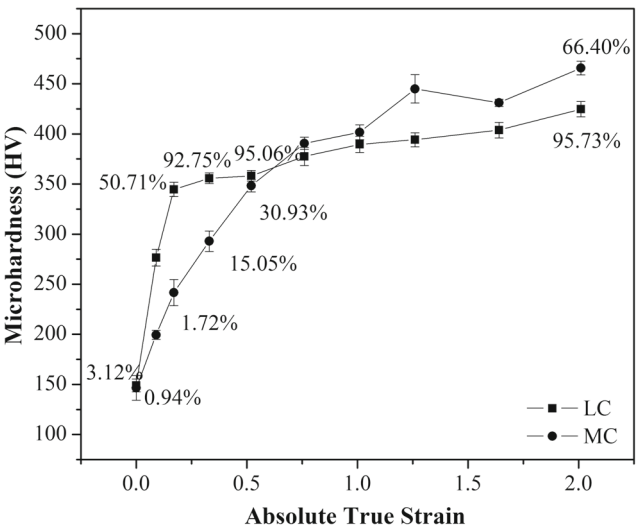

Fig. 13 Vickers microhardness versus absolute true strain for LC and MC alloys. MVF were inserted in some points of the curve

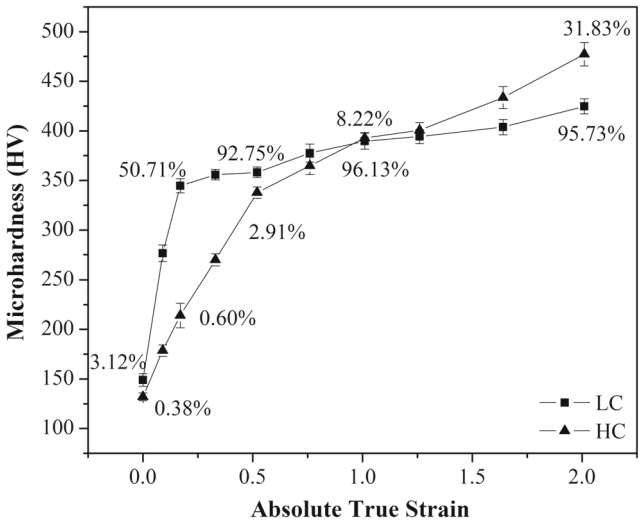

Fig. 14 Vickers microhardness versus absolute true strain for LC and HC alloys. MVF values were inserted in some points of the curve

Although the martensite content in each sample is different for the same amount of true strain, the strain hardening behavior reveals some interesting facts about how the chemical composition (i.e., austenite stability) affects the materials mechanical response. So, for a better interpretation, the volume fraction of austenite transformed into martensite was also inserted in these Figures. Initially, for the unstrained specimens, all microhardness values are very close to another, even though the mean value in the LC sample was slightly superior when compared to the HC. This result is a direct consequence of the much higher martensite content in the un-rolled LC, despite the fact that the HC steel has more carbon in solid solution. However, it is interesting to note that, in the LC alloy, the microhardness curves can be divided in two stages. The first stage relates to low strain levels, where the hardening effect is mainly due to phase transformation and strain hardening effects are less important. This behavior is supported by the fact that for equal amounts of true strain, before reaching the threshold, the LC alloy presents higher microhardness values than the MC and HC steels. Similar results were obtained by Tavares et al. [31, 33] in initial stages of true strain in AISI 304L, DSS UNS S31803 and AISI 201 Mod. The second stage, where the strain hardening effect is predominant, begins when a higher quantity of martensite is already present in the microstructure, and there is little change in the microhardness values due to transformation. Comparing with the LC alloy, the MC and HC microhardness curves also exhibit the same tendency to reach a similar threshold. However, it is important to note that for the MC alloy, the microhardness increase suggests a comparatively greater influence of work hardening in the early stage. This behavior stands out even more in the HC alloy, where the initial stage of hardness increase is almost exclusively due to work hardening effect.

4 Conclusions

The investigation about the influence of carbon content on the martensitic transformation of Ti-stabilized austenitic stainless steel (ASS) allows concluding:

The increase in carbon content also increases the stacking fault energy (SFE), resulting in a delayed $\gamma \rightarrow \alpha'$ transformation. The major fraction of the variation in the calculated SFE by thermodynamic model is due to the changes in carbon content.

The intrinsic saturation magnetization of martensite in AISI 321 ASS with low (LC), medium (MC), and high (HC) carbon content are 150.2, 134.3, and 120.2 Am^2/kg, respectively.

In the low carbon steel (LC), the micro-deformation process at the surface can induce the formation of ϵ martensite, due to a higher instability of austenite. A great amount of α' martensite is formed even at low strain levels.

Phase quantifications by X-ray diffraction (XRD) performed with different methodologies denoted texture and surface effects resulting from the polishing process in the low carbon ASS (LC) sample.

The kinetic behavior $\gamma \rightarrow \alpha'$ transformation of LC ASS is similar to AISI 301LN, while HC ASS is close to DSS UNS S31803. Also, the n and K parameters that define the transformation rate are very composition dependent.

The rate of martensitic transformation versus true strain curves presented in Fig. 12 leads to the conclusion that low SFE implies higher transformation rates at lower strain levels.

Finally, at initial cold rolling stages, the carbon content in Ti stabilized austenitic stainless steel alloys affect the main hardening mechanism, where the hardening process for low carbon contents is mainly governed by martensitic transformation. Thus, when carbon content increases, the work hardening effect becomes more predominant.

Funding information This study financially supported by the Brazilian research agencies CAPES, CNPq, and FAPERJ .

References

1. Nayyar ML (2000) Piping Handbook, 7th Ed. McGraw Hill, New York
2. Wright RN (2011) Other metallurgical systems for wire technology. Wire Technol:229–243. https://doi.org/10.1016/B978-0-12-382092-1.00015-4
3. Moss DR (1997) Pressure vessel design manual: Illustrated Procedures for Solving Major Pressure Vessel Design Problems

4. Hedayati A, Najafizadeh A, Kermanpur A, Forouzan F (2010) The effect of cold rolling regime on microstructure and mechanical properties of AISI 304L stainless steel. J Mater Process Technol 210:1017–1022. https://doi.org/10.1016/j.jmatprotec.2010.02.010
5. Ishimaru E, Hamasaki H, Yoshida F (2015) Deformation-induced martensitic transformation behavior of type 304 stainless steel sheet in draw-bending process. Journal of Mater Process Tech 223:34–38
6. Lu YQ, Hui H (2015) Investigation on mechanical behaviors of cold stretched and cryogenic stretched austenitic stainless steel pressure vessels. Procedia Eng 130:628–637. https://doi.org/10.1016/j.proeng.2015.12.282
7. Raj AK (2015) Formability: metastable austenitic stainless steels
8. Jha AK, Sivakumar D, Sreekumar K, Mittal MC (2008) Role of transformed martensite in the cracking of stainless steel plumbing lines. Eng Fail Anal 15:1042–1051. https://doi.org/10.1016/j.engfailanal.2007.11.012
9. Gomes da Silva MJ, Fragoso HAP, Barrio RCAG, Cardoso JL (2019) Stress corrosion of an austenitic stainless steel expansion joint, a case study. Eng Fail Anal 97:300–310. https://doi.org/10.1016/j.engfailanal.2019.01.021
10. Tiamiyu AA, Eskandari M, Nezakat M et al (2016) A comparative study of the compressive behaviour of AISI 321 austenitic stainless steel under quasi-static and dynamic shock loading. Mater Des 112:309–319. https://doi.org/10.1016/j.matdes.2016.09.087
11. Abreu HFGDH, Silva MMJG Da, Herculano LFG, Bhadeshia H (2009) Texture analysis of deformation induced martensite in an AISI 301L stainless steel: microtexture and macrotexture aspects. Mater Res 12:291–297. https://doi.org/10.1590/S1516-14392009000300008
12. Talonen J, Hanninen H (2007) Formation of shear bands and strain-induced martensite during plastic deformation of metastable austenitic stainless steels. Acta Mater 55:6108–6118. https://doi.org/10.1016/j.actamat.2007.07.015
13. Fargas G, Zapata A, Roa JJ et al (2015) Correlation between microstructure and mechanical properties before and after reversion of metastable austenitic stainless steels. Metall Mater Trans A 46:5697–5707. https://doi.org/10.1007/s11661-015-3178-8
14. Hadji M, Badji R (2002) Microstructure and mechanical properties of austenitic stainless steels after cold rolling. J Mater Eng Perform 11:145–151. https://doi.org/10.1361/105994902770344204
15. Behjati P, Najafizadeh A (2011) Role of chemical driving force in martensitic transformations of high-purity Fe-Cr-Ni alloys. Metall Mater Trans A Phys Metall Mater Sci 42:3752–3760. https://doi.org/10.1007/s11661-011-0769-x
16. Schramm RE, Reed RP (1975) Stacking fault energies of seven commercial austenitic stainless steels. Metall Trans A 6:1345–1351. https://doi.org/10.1007/BF02641927
17. Reed RP, Horiuchi T (1983) Austenitic steels at low temperatures. Springer, Boston
18. Das A (2016) Revisiting stacking fault energy of steels. Metall Mater Trans A Phys Metall Mater Sci 47:748–768. https://doi.org/10.1007/s11661-015-326
19. Yang SW, Spruiell JE (1982) Cold-worked state and annealing behaviour of austenitic stainless steel. J Mater Sci 17:677–690. https://doi.org/10.1007/BF00540364
20. Tsuchida N, Morimoto Y, Okamoto S et al (2008) Role of stress-induced martensitic transformation in TRIP effect of metastable austenitic stainless steels. Nippon Kinzoku Gakkaishi/Journal Japan Inst Met 72:769–775. https://doi.org/10.2320/jinstmet.72.769
21. Kang JH, Noh HS, Kim KM et al (2017) Modified Ni equivalent for evaluating hydrogen susceptibility of Cr-Ni based austenitic stainless steels. J Alloys Compd 696:869–874. https://doi.org/10.1016/j.jallcom.2016.12.061
22. Krupp U, Roth I, Christ HJ (2010) In situ SEM observation and analysis of martensitic transformation during short fatigue crack propagation in Metastable austenitic steel. Adv Eng Mater. https://doi.org/10.1002/adem.200900337
23. Moallemi M, Kermanpur A, Naja A et al (2016) Deformation-induced martensitic transformation in a 201 austenitic steel : the synergy of stacking fault energy and chemical driving force. Mater Sci Eng A 653:147–152
24. Saeedipour S, Kermanpur A, Najafizadeh A (2016) Effect of N on phase transformations during martensite thermomechanical processing of the nano/ultrafine-grained 201L steel. J Mater Eng Perform 25:5502–5512. https://doi.org/10.1007/s11665-016-2387-7
25. Curtze S, Kuokkala VT, Oikari A et al (2011) Thermodynamic modeling of the stacking fault energy of austenitic steels. Acta Mater 59:1068–1076. https://doi.org/10.1016/j.actamat.2010.10.037
26. de Dafe SSF, Sicupira FL, Matos FCS et al (2013) Effect of cooling rate on (ϵ, α') martensite formation in twinning/transformation-induced plasticity Fe-17Mn-0.06C steel. Mater Res 16:1229–1236. https://doi.org/10.1590/S1516-14392013005000129
27. Das A (2016) Revisiting stacking fault energy of steels. Metall Mater Trans A Phys Metall Mater Sci 47:748–768. https://doi.org/10.1007/s11661-015-3266-9
28. Ogawa T, Koyama M, Tasan CC et al (2017) Effects of martensitic transformability and dynamic strain age hardenability on plasticity in metastable austenitic steels containing carbon. J Mater Sci 52:7868–7882. https://doi.org/10.1007/s10853-017-1052-3
29. Beese AM, Mohr D (2011) Identification of the direction-dependency of the martensitic transformation in stainless steel using in situ magnetic permeability measurements. Exp Mech 51:667–676. https://doi.org/10.1007/s11340-010-9374-y
30. Shirdel M, Mirzadeh H, Parsa MH (2015) Estimation of the kinetics of martensitic transformation in austenitic stainless steels by conventional and novel approaches. Mater Sci Eng A 624:256–260. https://doi.org/10.1016/j.msea.2014.11.087
31. Tavares SSM, da Silva MR, Pardal JM et al (2006) Microstructural changes produced by plastic deformation in the UNS s31803 duplex stainless steel. J Mater Process Technol 180:318–322. https://doi.org/10.1016/j.jmatprotec.2006.07.008
32. Tavares SSM, Neto JM, da Silva MR et al (2008) Magnetic properties and α' martensite quantification in an AISI 301LN stainless steel deformed by cold rolling. Mater Charact 59:901–904. https://doi.org/10.1016/j.matchar.2007.07.007
33. Tavares SSM, Pardal JM, da Silva MJG et al (2009) Deformation induced martensitic transformation in a 201 modified austenitic stainless steel. Mater Charact 60:907–911. https://doi.org/10.1016/j.matchar.2009.02.001
34. Tavares SSM, Pardal JM, da Silva MR, de Oliveira CAS (2014) Martensitic transformation induced by cold deformation of lean duplex stainless steel UNS s32304. Mater Res 17:381–385. https://doi.org/10.1590/S1516-14392013005000157
35. Khatak HS (2002) 8 – Applications of fracture mechanics in stress corrosion cracking and introduction to life prediction approaches. In: Corrosion of Austenitic Stainless Steels. pp 190–217
36. Jafari E (2010) Corrosion behaviors of two types of commercial stainless steel after plastic deformation. J Mater Sci Technol 26:833–838. https://doi.org/10.1016/S1005-0302(10)60133-8
37. Moura V, Kina AY, Tavares SSM et al (2008) Influence of stabilization heat treatments on microstructure, hardness and intergranular corrosion resistance of the AISI 321 stainless steel. J Mater Sci 43:536–540. https://doi.org/10.1007/s10853-007-1785-5

38. Abedi F, Serajzadeh S (2018) Mechanical properties and strain-induced martensite transformation in cold rolling of 304L stainless steel plate. J Mater Eng Perform 27:6155–6165. https://doi.org/10.1007/s11665-018-3643-9
39. Jenkins R, Snyder RL, Robert L (1996) Introduction to X-ray powder diffractometry
40. Beese AM (2008) Quantification of phase transformation in stainless steel 301LN sheets. Massachusetts Institute of Technology
41. Cullity BD, Graham CD (2008) Introduction to magnetic materials. Wiley, Hoboken
42. Talonen J, Aspegren P, Hanninen H (2004) Comparison of different methods for measuring strain induced α'-martensite content in austenitic steels. Mater Sci Technol 20:1506–1512. https://doi.org/10.1179/026708304X4367
43. Rodríguez-Carvajal J (2001) Recent developments of the program FULLPROF. Int Union Crystallogr Newsl:12–19. https://doi.org/10.1007/s00603-013-0527-z
44. Belkly A, Helderman M, Karen VL, Ulkch P (2002) New developments in the inorganic Crystal Structure Database (ICSD): accessibility in support of materials research and design. Acta Crystallogr Sect B Struct Sci 58:364–369. https://doi.org/10.1107/S0108768102006948
45. Haušild P, Davydov V, Drahokoupil J (2010) Characterization of strain-induced martensitic transformation in a metastable austenitic stainless steel. Mater Des 31:1821–1827. https://doi.org/10.1016/j.matdes.2009.11.008
46. Plaut RL, Herrera C, Escriba DM (2007) A Short review on wrought austenitic stainless steels at high temperatures: processing, microstructure, properties and performance. Mater Res 10:453–460. https://doi.org/10.1590/S1516-14392007000400021